Formation of Intra-thermocline Lenses by Eddy-wind Interaction

Dennis J. McGillicuddy, Jr.
Woods Hole Oceanographic Institution, Woods Hole, Massachusetts

An expedited contribution revised and resubmitted to
Journal of Physical Oceanography

December 15, 2014

Corresponding author address: Dennis J. McGillicuddy, Jr., Department of Applied Ocean Physics and Engineering, Woods Hole Oceanographic Institution, Woods Hole, MA 02543, USA. Tel: 508-289-2683 Fax: 508-457-2194 Email: dmcgillicuddy@whoi.edu

Abstract

Mesoscale intra-thermocline lenses are observed throughout the world ocean, and are commonly attributed to water mass anomalies advected from a distant origin. An alternative mechanism of local generation is offered herein, in which eddy-wind interaction can create lens-shaped disturbances in the thermocline. Numerical simulations illustrate how eddy-wind driven upwelling in anticyclones can yield a convex lens reminiscent of a mode-water eddy, whereas eddy-wind driven downwelling in cyclones produces a concave lens that thins the mode-water layer (a cyclonic "thinny"). Such transformations should be observable with long term time-series in the interiors of mesoscale eddies.

1. Introduction

The mid-ocean is populated by a variety of different types of eddies. Most common are cyclones and anticyclones with vertical structures characteristic of the first baroclinic mode (Gill et al. 1974; McWilliams and Flierl 1976; Wunsch 1997), which tend to raise and lower the main thermocline, respectively (Fig. 1, left column). However, more complex vertical structures are not uncommon. Specifically, so-called "mode-water eddies" consist of a bolus of fluid that depresses the main thermocline and raises the seasonal thermocline (Fig. 1, upper right). Displacement of the main thermocline dominates both geostrophic velocity and sea level perturbations, such that these anticyclonic features are clearly detectable as positive sea level anomalies in satellite altimetry. The analogous second-baroclinic mode structure in the cyclonic case is upward displacement of the main thermocline and downward displacement of the seasonal thermocline, resulting in a thinning of the mode-water layer—thus the term "cyclonic thinny" (Fig. 1, lower right). Again the main thermocline signal dominates, and such cyclones are readily detectable as negative anomalies in sea level.

Two such eddies were the subject of detailed *in situ* process studies in the Sargasso Sea, mode-water eddy "A4", and cyclonic thinny "C1" (McGillicuddy et al. 2007). Both features had origins that could be traced back considerable distances from where they were sampled, as revealed by water mass analysis, transient tracer distributions, and backtracking of their trajectories via satellite altimetry (Jenkins et al. 2008; Li et al. 2008; McGillicuddy et al. 2007) . As such, their complex vertical structure is attributable at least in part to their non-local origins. In the case of A4, a bolus of mode water formed south of the Gulf Stream could have been subducted, subsequently penetrating into the Sargasso Sea as a mesoscale eddy (e.g., Ebbesmeyer and Lindstrom 1986). In the case of C1, there was a clear signature of subtropical

78 underwater (Schmitz and Richardson 1991) at eddy center in a thin stratum where mode water
79 was nearly absent; its water mass and biogeochemical characteristics suggest it may have been
80 advected from the southern Sargasso Sea (Li et al. 2008).
81 Despite the non-local contributions to the vertical structure of these two eddies, it is of
82 interest to discern whether or not the general sense of the isopycnal displacements could also be
83 explained by local forcing of the eddies themselves. Specifically, inclusion of the surface current
84 in calculation of the wind stress can yield mesoscale variations in Ekman divergence. That is,
85 higher stress occurs on the flank of the eddy where the wind opposes the surface current, with
86 lower stress on the flank of the eddy where the wind and the current are in the same direction.
87 The net result is Ekman suction (upwelling) in the interiors of anticyclones (Dewar and Flierl
88 1987; Martin and Richards 2001), and Ekman pumping (downwelling) in the interiors of
89 cyclones (Gaube et al. 2014a). This effect would tend to dome the seasonal thermocline in
90 anticyclones and depress it in cyclones, thus potentially transforming these features into intra-
91 thermocline lenses (Fig. 1). This idea is tested by comparing the results of idealized models of
92 isolated eddies forced by a standard wind stress formulation to those that include eddy-wind
93 interaction.
94
95 **2. Methods**
96 The Parallel Ocean Program (POP; Smith et al. 1992; Smith et al. 2000) was used for the
97 numerical experiments. This primitive equation model uses level coordinates and includes a free
98 surface. The configuration is the same as described in Ledwell et al. (2008). Specifically,
99 simulations are run in a 500 km^2 doubly-periodic domain with 2.88 km horizontal resolution.
100 The vertical grid has 72 levels, with resolution decreasing gradually from 5 m at the surface to

101 125 m at depth, and with the bottom located at 4462 m. Subgridscale horizontal mixing is
102 parameterized with a Laplacian operator of 1 m^2 s^{-1}. Vertical mixing is specified by the K-
103 profile method (Large et al. 1994) with a background diffusivity of 10^{-5} m^2 s^{-1} (Ledwell et al.
104 1993, 1998). In order to simplify diagnostics of the results in eddy-centric coordinates, the
105 model is configured on an f-plane to prevent the eddies from propagating.

106 Initial conditions (Fig. 2) consist of an isolated eddy at the center of the model domain.
107 Radially-symmetric temperature (*T*) and salinity (*S*) distributions are specified from average
108 profiles inside and outside the eddy of interest:

$$T(r,z) = T_{out}(z) + (T_{in}(z) - T_{out}(z))exp\left(-\frac{r^2}{r_0^2}\right)$$

$$S(r,z) = S_{out}(z) + (S_{in}(z) - S_{out}(z))exp\left(-\frac{r^2}{r_0^2}\right)$$

109 where r_0 is the eddy radius inferred from hydrographic data. Temperature and salinity surfaces
110 are assumed to be flat in the upper ocean ($z < 150$ m). This constitutes a departure from the
111 typical first baroclinic mode structure, but it facilitates clearer analysis of the disturbance of
112 near-surface isopycnals by eddy-wind interaction.

113 In order to prescribe velocities that are in approximate balance with the density field,
114 initial velocity fields are computed as the sum of geostrophic and cyclostrophic contributions,
115 assuming no motion at the bottom. The cyclostrophic terms constitute small corrections to the
116 geostrophic velocities. Modest adjustment of the interior velocity fields in the first few days of
117 the simulation attests to the efficacy of the initialization procedure.

118 Two runs were conducted for each eddy (Table 1): one with the standard wind stress (τ)
119 formulation:

$$\tau = \rho_{air} c_d u_{air} |u_{air}|$$

120 and one in which the stress is computed as the difference between air and ocean surface
121 velocities u_{air} and u_{sea}:

$$\tau = \rho_{air} c_d (u_{air} - u_{sea}) |u_{air} - u_{sea}|$$

122 where ρ_{air} is the density of air and c_d the drag coefficient, which is specified according to Large
123 and Pond (1981). The spatially-uniform wind has a speed of 6.7 m s^{-1}, which is characteristic of
124 summertime conditions in the region of the Sargasso Sea where eddies A4 and C1 were
125 observed. In order to preserve the radial and azimuthal symmetry of the simulated eddies, the
126 wind direction is assumed to rotate clockwise through a complete circle every 64 hours. The
127 specified period of wind rotation is somewhat arbitrary, although the key to maintaining
128 symmetry is a period short enough to prevent significant net Ekman transport in the horizontal
129 direction. A second consideration is avoiding resonance with the local inertial frequency (ca. 24
130 h). This *ad hoc* rotation of the wind vector successfully maintains eddy-centric symmetry in the
131 simulations, thereby simplifying the analysis.

132 In the absence of surface heating, wind forcing will cause deepening of the mixed layer.
133 In order to balance the input of turbulent kinetic energy by the wind, surface heat fluxes are
134 applied. A shortwave heat flux of 241 W m^{-2} into the ocean is specified (mean of shipboard
135 measurements, assuming a 4% albedo). Sensible, latent, and long-wave heat fluxes are
136 computed via bulk formulae. The resulting net heat flux is positive, thus maintaining a mixed
137 layer depth that is roughly consistent with the observations.

138

139 **3. Results**

140 After 100 days of integration in the anticyclonic case with the uniform wind stress
141 formulation, near-surface isopycnals remain flat as in the initial condition (Fig. 3a,b). The mixed

142 layer deepens due to the turbulence created by the wind stress, partially arrested by the decrease
143 in surface density due to the heat flux. In contrast, the run with eddy-wind interaction exhibits
144 upward doming of the near-surface isopycnals (Fig. 3c) as a result of upwelling at eddy center
145 and flow into the eddy interior at intermediate depths. At day 100, the magnitude of the
146 isopycnal displacements is comparable to those observed in eddy A4 (Fig. 3d). Note that the
147 simulation with eddy-wind interaction shows some shoaling of the depressed isopycnals in the
148 main thermocline (500-700 m) relative to the run without eddy-wind interaction, consistent with
149 findings that this mechanism accelerates eddy decay (Dewar and Flierl 1987; Eden and Dietze
150 2009; Zhai and Greatbatch 2007).

151 Similarly, in the cyclonic case, near-surface isopycnals remain flat in the simulation with
152 uniform wind stress (Fig. 4a,b). When the eddy-wind interaction effect is included, near-surface
153 isopycnals are deflected downward by convergence at eddy center, with flow out of the eddy at
154 intermediate depths causing thinning of the mode-water layer in the seasonal thermocline (Fig.
155 4c). This isopycnal topography is qualitatively similar to that observed, although the data
156 contain small-scale structure that is not represented in the model. As in the anticyclonic case,
157 eddy-wind interaction accelerates eddy decay, as evidenced by a reduction in the doming of
158 main-thermocline isopycnals.

159 In both the cyclonic and anticyclonic cases, the deflection of isopycnals associated with
160 eddy-wind interaction is relatively monotonic in time (not shown). This stems primarily from
161 the fact that the magnitude of the wind forcing is constant. However, because the eddies decay
162 over time, there is a slight decrease in the magnitude of the eddy-wind induced vertical velocity
163 (more details below), resulting in a slowing of isopycnal displacements during the simulation.

Inclusion of the surface currents in the wind stress formulation can also bring about spatial variations in mixing. Specifically, the input of turbulent kinetic energy is higher where the wind and the surface current oppose each other, and lower where the wind and surface current are in the same direction. However, the wind is constantly rotating in these simulations, thereby tending to smooth out such variations in the azimuthal direction. A more pronounced (but still modest) effect on mixed layer depth results from eddy/wind induced isopycnal displacements, with shallower (deeper) mixed layer depths inside the anticyclone (cyclone) where upwelling (downwelling) increases (decreases) stratification (Figs. 3c, 4c).

4. Discussion

The model results demonstrate that eddy-wind interactions can create intra-thermocline lenses with isopycnal topographies that are qualitatively similar to observations. However, it is important to note that congruence between the simulations and observations (Figs. 3, 4) reflects only a snapshot in time—if the simulations were run out over a longer period, one could expect continued increases in the amplitude of the upper ocean isopycnal displacements and decay of the main thermocline perturbations. Of course the time period of the simulations is rather arbitrary, especially in light of the idealized nature of the initial conditions in the upper ocean. It may be that at the time of eddy formation, upper ocean isopycnal displacements could have the same sense as those of the main thermocline (upward in cyclones and downward in anticyclones). In that case, it would take longer for the eddy transformations (standard anticyclone to mode-water eddy and standard cyclone to cyclonic thinny) to take place.

The simulated displacements of upper ocean isopycnals are consistent with vertical velocities w_E predicted by the scale analysis of Gaube et al. (2014b):

$$w_E = -\frac{3\rho_{air} c_d |u_{air}|}{2\rho_0 f}\zeta_{z=0}$$

where $\zeta_{z=0}$ is the relative vorticity of the eddy at the surface and ρ_0 is the density of water. With relative vorticities of ca. 0.1f, the expected vertical velocities at the base of the Ekman layers in A4 and C1 are on the order of 0.1 m d^{-1} for the specified wind conditions. This is sufficient to explain the rate at which upper ocean isopycnals are displaced in the simulations. As described in Dewar and Flierl (1987), the magnitude of the vertical motion decreases with depth from the base of of Ekman layer into the main thermocline, and thus the deeper isopycnals are disturbed less than those above.

In both cyclonic and anticyclonic cases, the deflection of upper ocean isopycnals creates geostrophic shear that is opposite in sign to that associated with the eddy-driven displacement of the main thermocline. This reduces the relative vorticity at the surface, thus decreasing the amplitude of the eddy/wind induced Ekman pumping w_E. This will continue until the relative vorticity at the surface goes to zero, presumably leaving an intra-thermocline lens intact, in which the upper ocean and main thermocline geostrophic shears exactly compensate each other at the surface.

5. Conclusions

This mechanism of local generation of intra-thermocline lenses constitutes a hypothesis in need of testing with observations. Long-term time-series within eddies are required to do so, and acquisition of such observations via shipboard surveys may prove to be impractical. Satellite data may be useful for this purpose, particularly given the utility of altimetry in eddy tracking (Chelton et al. 2011) and the capability to observe eddy/wind interaction in scatterometer measurements (Gaube et al. 2014b). Unfortunately, on the basis of sea level alone,

it is not possible to differentiate regular anticyclones from mode-water eddies, nor regular cyclones from cyclonic thinnies. Autonomous floats and gliders offer an attractive approach to monitoring long-term changes in the isopycnal topography within eddies, particularly if they could be strategically deployed in newly formed eddy features identified in satellite data. These observations could be synthesized in the context of additional numerical experiments, especially in more realistic settings than the idealized simulations described herein. Such a combination of models and observations would be ideally suited to investigating the formation of intra-thermocline lenses in the ocean, particularly in light of the intermittency of the underlying processes.

Acknowledgments

Support of this research by the National Science Foundation and National Aeronautics and Space Administration is gratefully acknowledged. I thank Bill Dewar for feedback during the initial analysis of the results, and Peter Gaube and John Marshall for comments that helped improve the manuscript. Larry Anderson carried out the model runs and provided technical assistance in figure preparation. The simulations were conducted on high-performance computers (ark:/85065/d7wd3xhc) provided by NCAR's Computational and Information Systems Laboratory, sponsored by the National Science Foundation.

References

Chelton, D. B., M. G. Schlax, and R. M. Samelson, 2011: Global observations of nonlinear mesoscale eddies. *Progress In Oceanography*, **91,** 167-216.

Dewar, W. K., and G. R. Flierl, 1987: Some effects of wind on rings. *Journal of Physical Oceanography*, **17,** 1653-1667.

Ebbesmeyer, C. C., and E. J. Lindstrom, 1986: Structure and origin of 18C water observed during the POLYMODE Local Dynamics Experiment. *Journal of Physical Oceanography*, **16,** 443-453.

Eden, C., and H. Dietze, 2009: Effects of mesoscale eddy/wind interactions on biological new production and eddy kinetic energy. *Journal of Geophysical Research*, **114,** C05023.

Gaube, P., D. J. McGillicuddy, D. B. Chelton, M. J. Behrenfeld, and P. G. Strutton, 2014a: Regional variations in the influence of mesoscale eddies on near-surface chlorophyll. *Journal of Geophysical Research: Oceans***,** in press.

Gaube, P., D. B. Chelton, R. M. Samelson, M. G. Schlax, and L. W. O'Neill, 2014b: Satellite Observations of Mesoscale Eddy-Induced Ekman Pumping. *Journal of Physical Oceanography***,** in press.

Gill, A. E., J. S. A. Green, and A. J. Simmons, 1974: Energy partition in the large-scale ocean circulation and the production of mid-ocean eddies. *Deep-Sea Research*, **21,** 499-528.

Jenkins, W. J., D. J. McGillicuddy, and D. E. Lott, 2008: The distributions of, and relationship between, 3He and nitrate in eddies. *Deep-Sea Research II*, **55,** 1389-1397.

Large, W. G., and S. Pond, 1981: Open ocean momentum flux measurements in moderate to strong winds. *Journal of Physical Oceanography*, **11,** 329-336.

Large, W. G., J. C. McWilliams, and S. C. Doney, 1994: An oceanic vertical mixing scheme with a k-profile boundary layer parameterization. *Rev. Geophys.*, **32,** 363-403.

Ledwell, J. R., A. J. Watson, and C. S. Law, 1993: Evidence for slow mixing across the pycnocline from an open-ocean tracer-release experiment. *Nature*, **364,** 701-703.

——, 1998: Mixing of a tracer released in the pycnocline. *Journal of Geophysical Research*, **103,** 21,499-421,529.

Ledwell, J. R., D. J. McGillicuddy, and L. A. Anderson, 2008: Nutrient flux into an intense deep chlorophyll layer in a mode-water eddy. *Deep-Sea Research II*, **55,** 1139-1160.

Li, Q. P., D. A. Hansell, D. J. McGillicuddy, Jr., N. R. Bates, and R. J. Johnson, 2008: Tracer-based assessment of the origin and biogeochemical transformation of a cyclonic eddy in the Sargasso Sea. *Journal of Geophysical Research*, **113,** C10006.

Martin, A. P., and K. J. Richards, 2001: Mechanisms for vertical nutrient transport within a North Atlantic mesoscale eddy. *Deep-Sea Research II*, **48,** 757-773.

McGillicuddy, D. J., and Coauthors, 2007: Eddy/wind interactions stimulate extraordinary mid-ocean plankton blooms. *Science*, **316,** 1021-1026.

McWilliams, J. C., and G. R. Flierl, 1976: Optimal quasigeostrophic wave analysis of MODE array data. *Deep-Sea Research*, **23,** 285-300.

Schmitz, W. J., and P. L. Richardson, 1991: On the sources of the Florida Current. *Deep-Sea Research*, **38, Supplement 1,** S379-S409.

Smith, R. D., J. K. Dukowicz, and R. C. Malone, 1992: Parallel ocean circulation modeling. *Physica D*, **60,** 38-61.

Smith, R. D., M. E. Maltrud, F. O. Bryan, and M. W. Hecht, 2000: Numerical simulation of the North Atlantic Ocean at 1/10 degree. *Journal of Physical Oceanography*, **30,** 1532-1561.

Wunsch, C., 1997: The vertical partition of horizontal kinetic energy. *Journal of Physical Oceanography*, **27,** 1770-1794.

Zhai, X., and R. J. Greatbatch, 2007: Wind work in a model of the northwest Atlantic Ocean. *Geophysical Research Letters*, **34,** L04606.

Run	Eddy	Wind stress
1	A4	$\tau = \rho_{air} c_d u_{air} \lvert u_{air} \rvert$
2	A4	$\tau = \rho_{air} c_d (u_{air} - u_{sea}) \lvert u_{air} - u_{sea} \rvert$
3	C1	$\tau = \rho_{air} c_d u_{air} \lvert u_{air} \rvert$
4	C1	$\tau = \rho_{air} c_d (u_{air} - u_{sea}) \lvert u_{air} - u_{sea} \rvert$

Table 1. Summary of numerical simulations.

Figure Captions

FIG 1. Hypothesized transformations of a regular anticyclone into a mode-water eddy (top) and a regular cyclone into a cyclonic "thinny" (bottom). Each cross-section depicts an isopycnal in the seasonal (ρ_1) and main thermocline (ρ_2).

FIG. 2. Initial conditions for an idealized anticyclone with downward displacement of the main thermocline similar to that of mode-water eddy A4. (A) Depth of the σ_θ=27.0 isopycnal; (B) azimuthal velocity. Corresponding initial conditions for cyclone C1 are not shown. See Figs. 3a and 4a for vertical sections of density in the initial conditions for A4 and C1, respectively.

FIG. 3. Simulated and observed cross-sections. (A) Initial condition for an anticyclonic eddy with main thermocline displacement similar to mode-water eddy A4 and flat near-surface isopycnals. (B) and (C): Results after 100 days of integration without and with eddy-wind interaction, respectively. (D) Observed cross section of mode-water eddy A4.

FIG. 4. Simulated and observed cross-sections. (A) Initial condition for a cyclonic eddy with main thermocline displacement similar to cyclonic thinny C1 and flat near-surface isopycnals. (B) and (C): Results after 100 days of integration without and with eddy-wind interaction, respectively. (D) Observed cross section of cyclonic thinny C1.

306 FIG. 1. Hypothesized transformations of a regular anticyclone into a mode-water eddy (top) and
307 a regular cyclone into a cyclonic "thinny" (bottom). Each cross-section depicts an isopycnal in
308 the seasonal (ρ_1) and main thermocline (ρ_2).
309

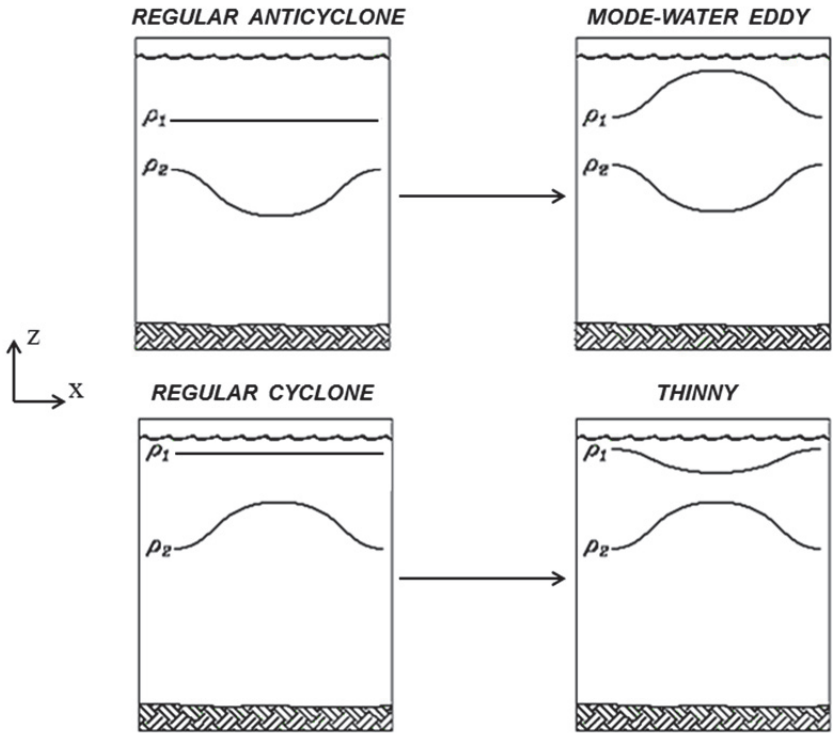

310
311
312

FIG. 2. Initial conditions for an idealized anticyclone with downward displacement of the main thermocline similar to that of mode-water eddy A4. (A) Depth of the σ_θ=27.0 isopycnal; (B) azimuthal velocity. Corresponding initial conditions for cyclone C1 are not shown. See Figs. 3a and 4a for vertical sections of density in the initial conditions for A4 and C1, respectively.

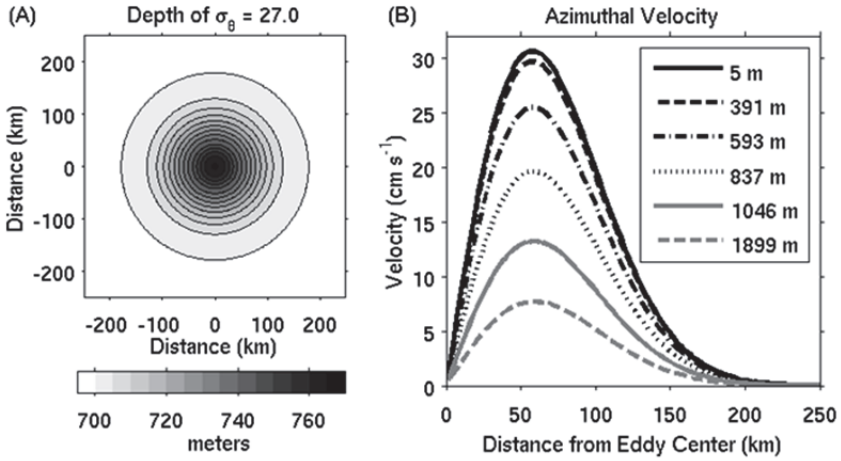

FIG. 3. Simulated and observed cross-sections. (A) Initial condition for an anticyclonic eddy with main thermocline displacement similar to mode-water eddy A4 and flat near-surface isopycnals. (B) and (C): Results after 100 days of integration without and with eddy-wind interaction, respectively. (D) Observed cross section of mode-water eddy A4.

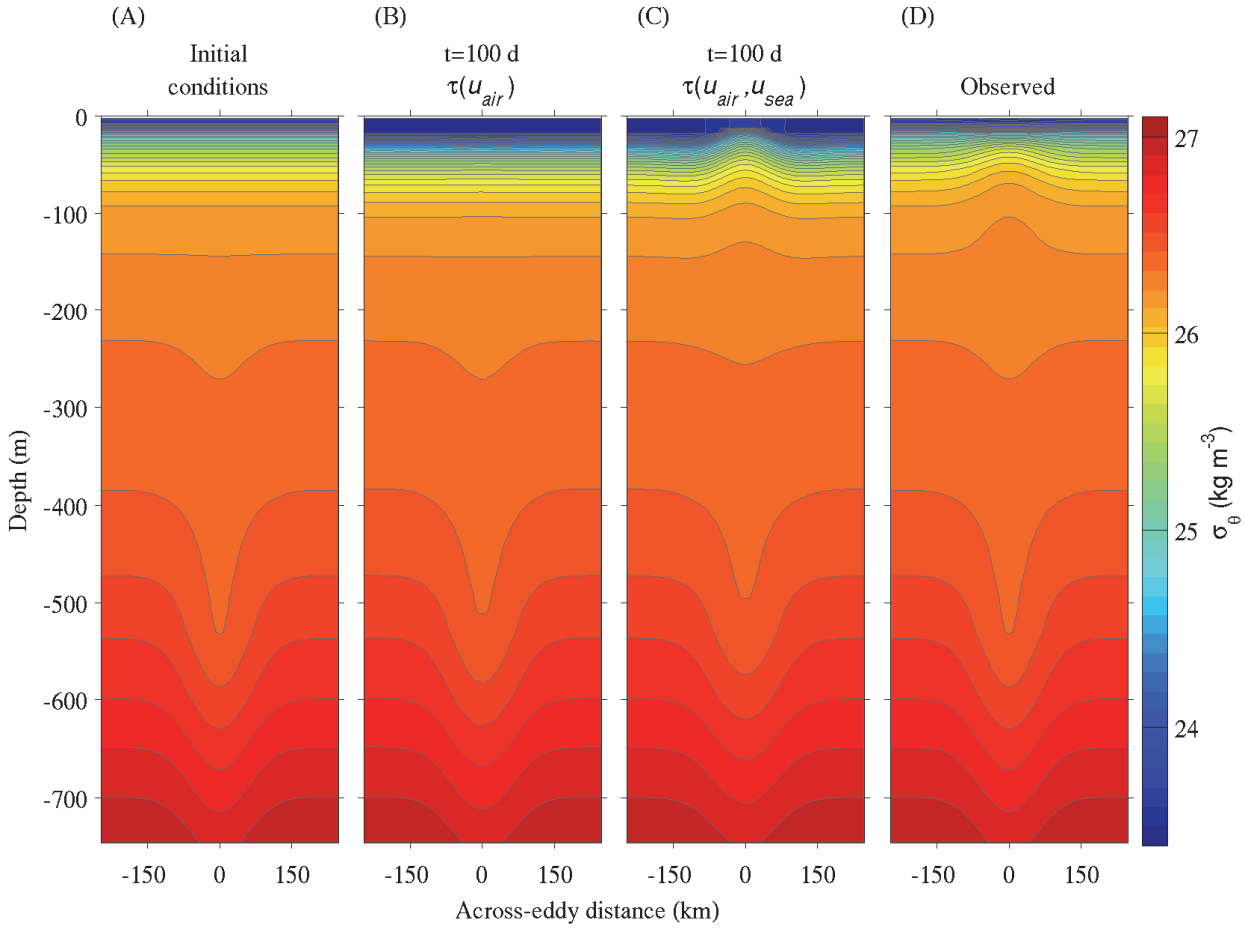

FIG. 4. Simulated and observed cross-sections. (A) Initial condition for a cyclonic eddy with main thermocline displacement similar to cyclonic thinny C1 and flat near-surface isopycnals. (B) and (C): Results after 100 days of integration without and with eddy-wind interaction, respectively. (D) Observed cross section of cyclonic thinny C1.